



Electrochemical characterization of the brownmillerite $\text{Ca}_2\text{Fe}_2\text{O}_{5+\delta}$ synthesized by citrate sol–gel method. Application to photocatalytic H_2 -production

S. Benallal¹ · S. Boumaza¹ · R. Brahimi² · M. Trari²

Received: 1 July 2021 / Revised: 28 April 2022 / Accepted: 4 May 2022 / Published online: 21 May 2022
© The Author(s), under exclusive licence to Springer-Verlag GmbH Germany, part of Springer Nature 2022

Abstract

The present study focuses on the preparation and electrochemical characterization of the calcium ferrite ($\text{Ca}_2\text{Fe}_2\text{O}_{5+\delta}$), a semiconductor crystallizing in the brownmillerite structure. The oxygen over-stoichiometry δ is extended to 0.16. It was synthesized by sol–gel auto combustion using nitrates as precursors and citric acid as chelating agent. The X-ray diffraction and specific surface area analysis showed a single phase with a specific surface area of $\sim 6 \text{ m}^2 \text{ g}^{-1}$. The optical gap of $\text{Ca}_2\text{Fe}_2\text{O}_5$ ($E_g = 2.31 \text{ eV}$), determined by the diffuse reflectance spectroscopy, is assigned to $d-d$ transition of Fe^{3+} : $3d$ orbital in octahedral coordination. It enables the photocatalytic exploitation of a large part of the solar spectrum. The p -type behavior of the oxide was demonstrated by photo-electrochemistry with an electro affinity of 3.69 eV ($\pm 0.20 \text{ eV}$). A flat band potential ($E_{\text{fb}} = 0.93 \text{ V}_{\text{SCE}}$) was evaluated from the capacitance-potential ($C^{-2}-E$) characteristic while the holes density ($N_A = 2.63 \times 10^{16} \text{ cm}^{-3}$) was determined from the thermo-power $S_{300\text{K}} (= 1.1 \text{ mV K}^{-1})$. The electrochemical oxygen intercalation is evidenced from the intensity-potential ($J-E$) profile. The semicircle in the Nyquist diagram is assigned to the bulk contribution whose diameter ($233 \text{ k}\Omega \text{ cm}^2$) decreases down to $203 \text{ k}\Omega \text{ cm}^2$ under illumination, thus confirming the semi conductivity of the brownmillerite. The cathodic potential of the conduction band (CB) showed the feasibility of the water reduction. Indeed, $\text{Ca}_2\text{Fe}_2\text{O}_5$ with a good chemical stability over a large pH range (5–14) was positively tested as photocatalyst for the H_2 production upon visible light. The best activity was observed in alkaline medium (NaOH, 10^{-3} M) with an average evolution rate of $0.07 \text{ cm}^3 \text{ h}^{-1} (\text{mg catalyst})^{-1}$ under a light flux of 29 mW cm^{-2} .

Keywords Brownmillerite $\text{Ca}_2\text{Fe}_2\text{O}_5$ · Sol–gel auto combustion · Hydrogen · Photocatalysis · Visible light

Introduction

Ternary oxides are widely employed in the solar energy conversion and continue to attract a growing interest because of their low cost, chemical stability, and facile preparation. Therefore, the search of new photocatalysts has been particularly focused on inorganic semiconductors (SC) for the

photo-electrochemical (PEC) conversion of light to useful energies [1] and the perovskite-derived compounds remain privileged as electro-catalysts [2, 3] and photocatalysts [4, 5]. Among the oxides, the brownmillerites with the general formula $\text{A}_2\text{B}_2\text{O}_5$ ($\text{A} = \text{Ca}, \text{Sr}$, and $\text{B} = \text{Fe}, \text{Al}, \text{Co}$) display a high ionic conductivity owing to its two-dimensional character and found applications in Li-ion batteries [6] and photocatalysis [7]. They are related to the perovskite (ABO_3) structure by introduction of an ordered array of oxygen vacancies with alternate layers of octahedrally and tetrahedrally coordinated metal [8]. This structure allows the accommodation of $3d$ cations of different valences with the capacity to support various types of defects [9], and the origin of the photocurrent comes from the electronic excitation from the valence band to acceptor levels. Most ferrite oxides exhibit a semiconductor behavior, absorb in the visible region with a band gap of $\sim 2 \text{ eV}$, and possess a

✉ S. Benallal
sbenallal@usthb.dz

✉ S. Boumaza
boumzasouhila@gmail.com

¹ Laboratory of Chemistry of Natural Gas, Faculty of Chemistry (USTHB), BP 32, 16111 Algiers, Algeria

² Laboratory of Storage and Valorisation of Renewable Energies, Faculty of Chemistry (USTHB), BP 32, 16111 Algiers, Algeria

cathodic conduction band; such characteristics are required in photocatalysis [10, 11].

Indeed, the main hindrance limiting the photoelectrochemical performance of the semiconducting materials is the large optical gap. $\text{Ca}_2\text{Fe}_2\text{O}_5$ is an anion-deficient perovskite with a narrow gap (E_g) formed from abundant elements where both iron and calcium are available and nontoxic. It exhibits p -type behavior and possesses a cathodic conduction band and a high reducing ability [12, 13]. However, there are fewer reports in the literature on its electrochemical and photocatalytic properties [14]. $\text{Ca}_2\text{Fe}_2\text{O}_5$ is characterized photo-electrochemically to evaluate its activity as bias-free H_2 photocathode since the conduction band (CB) is more cathodic than the $\text{H}_2\text{O}/\text{H}_2$ level. However, it does not correspond to the redox level required for water separation due to the high oxygen overvoltage, which exceeds 1 V and therefore a hole scavenger is necessary to close the electrical circuit and prevent photocorrosion [15].

Experimental

The sol–gel auto combustion method was used to prepare the brownmillerite; $\text{Ca}(\text{NO}_3)_2 \cdot 4\text{H}_2\text{O}$ (Panreac, 98.5%) and $\text{Fe}(\text{NO}_3)_3 \cdot 9\text{H}_2\text{O}$ (Scharlau, 99%) were used as precursors with a molar ratio (1/1). They were dissolved in distilled water to which citric acid was added dropwise; then, the solution was evaporated in a Rota vapor under vacuum. The resulting gel was denitrified at 300 °C in a ventilated place until total disappearance of NO_x fumes; the powder was ground in an agate mortar and fired at 800 °C (5 °C min^{-1}), naturally cooled to room temperature, and stored in a desiccator.

The phase was identified with a XPERT-PRO diffractometer using a monochromatic Cu K_α line ($\lambda = 0.15406$ nm). The crystallite dimension was calculated from the full width at half maximum of the strongest XRD peak. The specific surface area was determined by the BET method on ASAP2010 micromeritics equipment using N_2 gas as adsorbent at 77 K. The diffuse reflectance data were collected with a Jasco 650 UV–VIS spectrophotometer fitted to an integration sphere; PTFE was used as reference. The morphology of the oxide was visualized by scanning electron microscopy (SEM) using a JSM Jeol 6360L microscope.

Pellets (thickness ~ 2 mm) were obtained by compacting the powder under a pressure of 5 kbar and annealed at 800 °C, yielding a relative density of 90% with good mechanical properties. The pellets were introduced in glass tubes and isolated with the hardening araldite. For the ohmic contact, a copper wire was fixed on one face of the electrode using silver cement. The front active surface was polished with fine emery papers and thoroughly washed with water before use. The electrochemical characterization was

realized at ambient temperature in NaOH solution (Biochem, 98%, 10^{-3} M). A conventional three-electrode set-up was used with the reference SCE, Pt counter-electrode (0.5 cm^2), and the working electrode (0.38 cm^2). The interfacial capacitance was measured as a function of potential with a PGZ301 potentiostat/galvanostat, AC voltage signal of 10 kHz in frequency, and 10 mV peak to peak in magnitude were used. An inert atmosphere was ensured by bubbling pure N_2 gas through the solution. The complex impedance data were recorded with small amplitude wave signals in the range (10^{-2} – 10^5 s^{-1}).

The incorporation of O^{2-} species in the crystal lattice implies the formation of Fe^{4+} as required by the electro-neutrality condition: $\text{Ca}_{2-2\tau}\text{Fe}_{2+2\tau}\text{Fe}^{4+}\text{O}_{5+\tau/2}$. The concentration of Fe^{4+} ion was analyzed using the Mohr salt according the redox process: $\text{Fe}^{2+} + \text{Fe}^{4+} \rightarrow 2\text{Fe}^{3+}$. The remaining Fe^{2+} is back titrated by KMnO_4 , and τ is given by:

$$\tau = \frac{M N \Delta V}{m - 8 N \Delta V} \quad (1)$$

where M is the molar weight of $\text{Ca}_2\text{Fe}_2\text{O}_5$, m the mass of dissolved sample, N the normality of KMnO_4 (10^{-2} N), and ΔV the difference between the volume consumed and the blank test. A formulation $\text{Ca}_{2+2\tau}\text{Fe}_{2-2\tau}\text{Fe}^{4+}\text{O}_{5-\tau/2}$ is determined ($\tau=0.32$).

The photoactivity was assessed by measuring the evolved H_2 volume under visible light, provided by three tungsten-halogen lamps in a device described elsewhere [16]. Hydrogen was identified by gas chromatography (Agilent Technology 7890A). Because its H_2 has weak solubility in water, its volume was collected by liquid displacement in a graduated burette with a small internal diameter for a higher sensitivity. All solutions were prepared from reagents of analytical quality and distilled water (~ 0.8 MΩ cm).

Results and discussion

Structural properties

The XRD pattern of $\text{Ca}_2\text{Fe}_2\text{O}_5$ calcined at 800 °C (Fig. 1) is characteristic of a single-phase crystallizing in the brownmillerite structure. All peaks are indexed in an orthorhombic symmetry (Space Group: Pnma) in agreement with the JCPDS Card No. 47–1744; the lattice constants: $a = 5.431(5)$ Å, $b = 14.763(9)$ Å, and $c = 5.601(4)$ Å were refined by the least square method; a slight discrepancy is noticeable with the literature due to the oxygen over-stoichiometry. The brownmillerite contains oxygen vacancy row which functions as channels for oxygen diffusion between tetrahedral layers. Indeed, the additional oxygen ions, determined by chemical titration through the analysis of Fe^{4+} , are disorderly

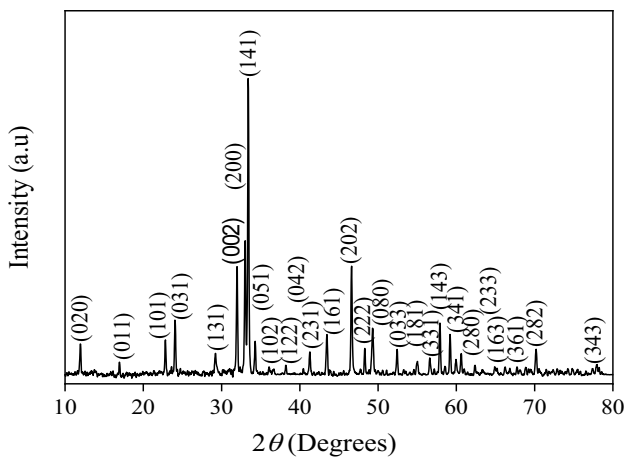


Fig. 1 Powder X-ray diffraction pattern of the brownmillerite $\text{Ca}_2\text{Fe}_2\text{O}_5$ prepared by sol–gel and calcined at 800°C

distributed; this is deduced from the fact that the diffractogram is satisfactory indexed in a non-stoichiometric perovskite since any long-range ordering should produce peaks associated with the super-lattice.

The crystallite size ($D \sim 55$ nm) was calculated from the broadening of the strongest XRD peak (β , rad.): $D = 0.9 \lambda (\beta \cos\Theta)^{-1}$. An active surface area of $6 \text{ m}^2 \text{ g}^{-1}$ was determined experimentally by the BET method; the surface area and the total pore volume ($0.0113 \text{ cm}^3/\text{g}$) of $\text{Ca}_2\text{Fe}_2\text{O}_5$ are relatively small, due to the calcination temperature (800°C).

The SEM micrograph (Fig. 2) shows a homogeneous microstructure with an agglomeration of irregular and shaped particles. The porous surface of the solid was activated by the gases evolution (CO_2 and NO_x) escaping from the gel during the combustion and resulting in grain spraying and pore formation [17].

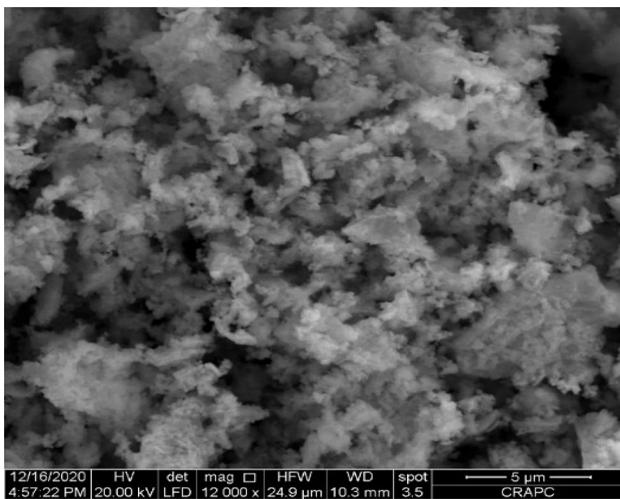


Fig. 2 The SEM image of $\text{Ca}_2\text{Fe}_2\text{O}_5$ prepared by sol–gel route

Optical and electrical properties

Most ferrites oxides are colored and absorb over the visible light due to their narrow band gap (< 2.5 eV) [18]. The optical gap (E_g) and the band edges position of $\text{Ca}_2\text{Fe}_2\text{O}_5$ are crucial in photocatalysis. The diffuse reflectance spectrum (Fig. 3) shows a broad absorption at 536 nm, a value consistent with the brown color of the powder. The optical transition of the semiconductor is accurately obtained from the relation [19]:

$$(\alpha h\nu)^n = \text{Const} \times (h\nu - E_g) \quad (2)$$

The exponent n is equal to 2 or 0.5 respectively for direct or indirect allowed transitions. The intersection of the linear part $(\alpha h\nu)^2$ plot with the $h\nu$ -axis gives a direct transition at 2.31 eV.

The oxygen crystal field splits the $\text{Fe}^{3+} 3d$ orbital in six-fold coordination and the gap E_g of $\text{Ca}_2\text{Fe}_2\text{O}_5$ is correlated to the internal transition $t_{2g} \rightarrow e_{2g}$.

Generally, the layered perovskite accommodates oxygenated species with a charge compensation mechanism [20]. Indeed, the positive thermo-power ($S_{300\text{K}} = 1.1 \text{ mV K}^{-1}$), measured at room temperature, confirms the p -type conduction of $\text{Ca}_2\text{Fe}_2\text{O}_5$ with holes as majority carriers:

$$S = \left(\frac{k}{e}\right) \ln\left(\frac{N_o}{N_A}\right) \quad (3)$$

Such character is due to oxygen insertion between the layers of FeO_6 octahedra sharing corners. The concentration of available sites N_o ($= 9.1 \times 10^{21} \text{ cm}^{-3}$) is calculated from the experimental density. The S value gives a density of effective free holes N_A of $2.63 \times 10^{16} \text{ cm}^{-3}$, and a mobility μ_h ($= 2.78 \times 10^{-7} \text{ cm}^2 \text{ V}^{-1} \text{ s}^{-1}$), calculated from

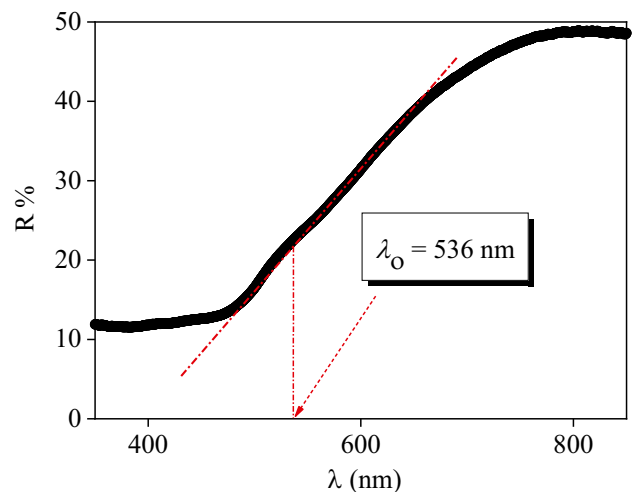


Fig. 3 Diffuse reflectance spectrum of $\text{Ca}_2\text{Fe}_2\text{O}_5$

the formula ($\sigma = e N_A \mu_h$). The hole conduction is associated with Fe^{3+} cations, forming small polaron lattice with a fraction of Fe^{4+} cations resulting from $\text{Ca}_2\text{Fe}_2\text{O}_{5+\delta}$ by the electro-neutrality condition [21, 22]. The mixed $\text{Fe}^{4+/3+}$ valences facilitate the charge transport [23, 24] and the hole-type conduction is explained by the O^{2-} insertion according to the following reaction [20]:

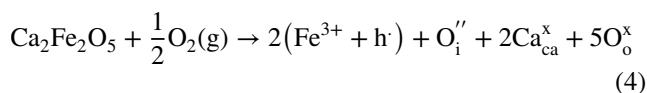
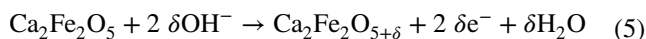


Photo-electrochemistry

$\text{Ca}_2\text{Fe}_2\text{O}_5$ is an interesting material for the PEC characterization and the appropriate position of the electronic bands makes it important to explore. The voltammogram $J(E)$ recorded in the dark in NaOH solution (pH ~ 11) shows a small current density ($< 0.2 \text{ mA cm}^{-2}$) over a wide potential range (Fig. 4) attributed to the thermal excitation from the valence band to acceptor levels, which overcomes the activation energy of electron hopping. The decrease in current below $\sim -0.7 \text{ V}$ is attributed to the evolution of H_2 as evidenced by the release of gas bubbles. The diffusion plateaus, before the water oxidation corresponds to oxygen insertion in the layered crystal according to the reaction:



The $J(E)$ characteristic plotted upon irradiation shows that the photocurrent J_{ph} augments in the cathodic direction (Fig. 4 inset), supporting the p -type semi-conductivity according to the Gartner model:

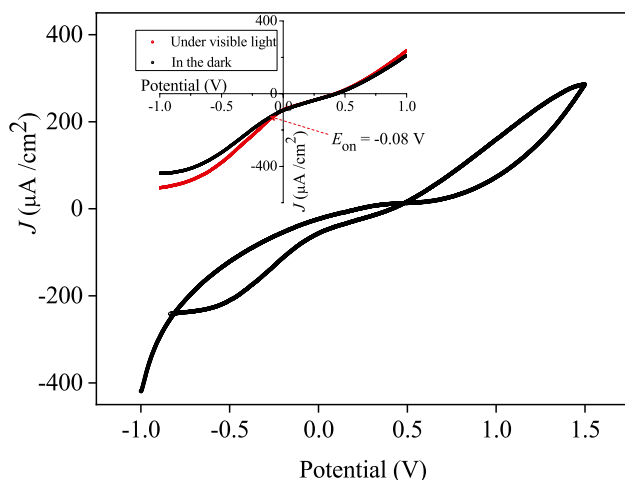


Fig. 4 Cyclic $J(E)$ characteristic of $\text{Ca}_2\text{Fe}_2\text{O}_5$ in NaOH (10^{-3} M) solution inset: The $J(E)$ plots in the dark and upon illumination

$$j_{\text{ph}}^2 = \text{const} \alpha^2 \delta^2 (E - E_{\text{on}}) \quad (6)$$

The photocurrent onset potential ($E_{\text{on}} = -0.08 \text{ V}$) for which J_{ph} appears is deduced from the cross point of the line $J_{\text{ph}}^2(E)$ with the potential axis (Fig. 5 inset). The chronoamperometric profile of the electrode polarized at -0.5 V , i.e., the variation of the current density (J) against the time under light (SM 1) supports the p -type conduction of $\text{Ca}_2\text{Fe}_2\text{O}_5$ with the oxidation of Fe^{3+} to Fe^{4+} ; the quantity of Fe^{4+} ($\tau = 0.32$) can be quantified by coulometry.

The charge involved in the cyclic voltammetry averages $\sim 10^{20}$ carriers cm^{-3} assuming a homogeneous oxygen distribution. The electro-kinetic parameters are derived from the semi-logarithmic plot (SM 2): the low exchange current density ($24 \mu\text{A cm}^{-2}$) and the high polarization resistance ($4.09 \text{ k}\Omega \text{ cm}^2$) confirm the electrochemical stability of the oxide in the working solution (pH ~ 11).

In the absence of sub-band gap states, the potential E_{on} can be reasonably assimilated to the flat band potential (E_{fb}). However, the latter is reliably obtained from the capacitance dependence (Fig. 5) on the applied potential ($C^{-2}-E$) according to the well-known relation [25]:

$$\frac{1}{C^2} = \frac{2}{e\epsilon\epsilon_0 N_A} (E - E_{\text{fb}}) \quad (7)$$

where e and ϵ_0 are the electronic charge and dielectric constant of vacuum respectively. The data were collected at 10 kHz to evaluate the potential E_{fb} ; such frequency is high enough to eliminate the parasite capacitances. The dielectric constant of $\text{Ca}_2\text{Fe}_2\text{O}_5$ ($\epsilon \sim 45$) was determined experimentally from the capacitance measurement on sintered pellet. The line ($C^{-2}-E$) is negatively sloped and corroborates the

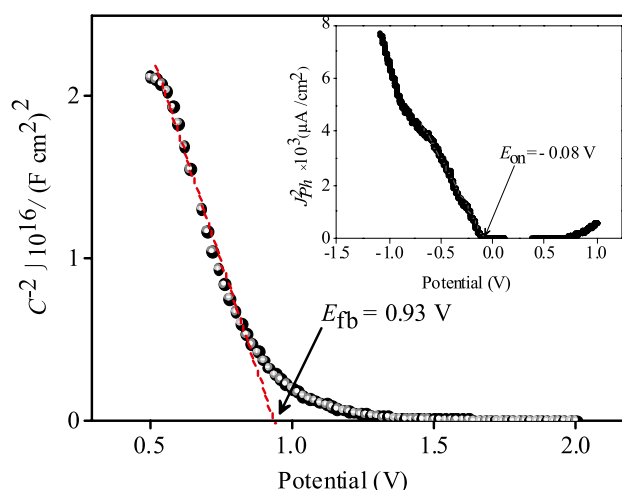


Fig. 5 ($C^{-2}-E$) characteristic of $\text{Ca}_2\text{Fe}_2\text{O}_5$ plotted in NaOH (10^{-3} M) solution. Inset the photocurrent onset potential determined according to the Gartner model

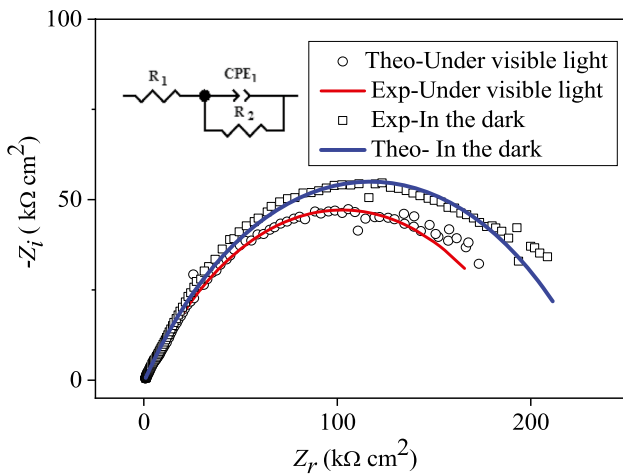


Fig. 6 The EIS diagram of $\text{Ca}_2\text{Fe}_2\text{O}_5$ in NaOH (10^{-3} M) electrolyte

p -type character of $\text{Ca}_2\text{Fe}_2\text{O}_{5+\delta}$. The intersection with the potential axis gives a potential E_{fb} ($=0.93$ V), more positive than the potential E_{on} (~ -0.08 V) and the large difference indicates the existence of surface states within the gap region.

The PEC characterization enables us to establish an energy diagram (Fig. 7) which predicts from a thermodynamic point of view whether the evolution of H_2 is feasible or not. The potential of the couple $\text{H}_2/\text{H}_2\text{O}$ depends on the pH and is determined by the intersection of the tangent of the cathodic branch with the potential axis in the J-E curve, a value of ~ -0.7 V is determined in NaOH medium. The potential E_{fb} relates the physical and electrochemical scales according to the basic equation in photo-electrochemistry ($Q = |e| [4.75 - E_{red}]$). $\text{Ca}_2\text{Fe}_2\text{O}_5\text{-CB}$ ($E_{CB} = -1.06$ V) is more cathodic than the $\text{H}_2\text{O}/\text{H}_2$ level and should lead to

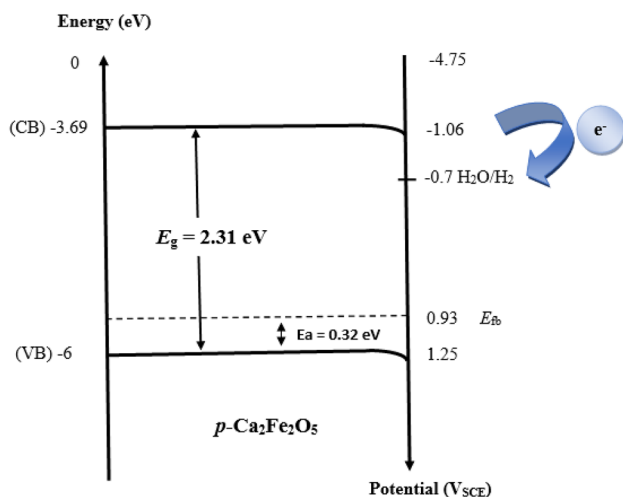


Fig. 7 The energy diagram of the junction $\text{Ca}_2\text{Fe}_2\text{O}_5 / \text{NaOH}$ (10^{-3} M)

H_2 evolution under visible light. The position of the valence band ($E_{VB} = 1.25$ V) is deduced from the relation:

$$P = E_a + |e| \times E_{fb} \tag{8}$$

As mentioned above, the brownmillerite is interesting to study electrochemically because of the suitable position of the electronic bands. When the light is on, the holes are no longer ionized and the stability is likely to be improved by the p -type nature of $\text{Ca}_2\text{Fe}_2\text{O}_5$. The low dark current yields an extended space charge region ($W \sim 310$ nm) resulting from the density N_A ; the width W is computed for an optimal band bending ($\Delta U = 0.5$ V) using the formula:

$$W = \left[\frac{2\epsilon\epsilon_0\Delta U}{eN_A} \right]^{0.5} \tag{9}$$

The EIS analysis is a reliable technique for quantifying the electron transfer at the solid/electrolyte junction and allows elucidating the interfacial reactions. The complex diagrams of $\text{Ca}_2\text{Fe}_2\text{O}_5$ plotted in the obscurity and under visible light at the free potential are illustrated in Fig. 6. As expected, the diameter of the depressive semicircle at high frequency (233 $\text{k}\Omega \text{ cm}^2$), assigned to the charge transfer (R_{ct}), decreases down to 203 $\text{k}\Omega \text{ cm}^2$ under illumination, corroborating the semi conductivity of the brownmillerite. The absence of inclined line at low frequencies (Warburg diffusion) indicates that the electron transfer within the depletion zone is rate determining. The shift from the origin corresponds to the electrolytic solution ($R_{el} = 430$ $\Omega \text{ cm}^2$), due to the ionic electrolyte (Na^+, OH^-). An electrical equivalent circuit (Fig. 6) models suitably the EIS data. The porous nature, the roughness, and heterogeneity of the electrode surface as well as the sub band states in the gap region of $\text{Ca}_2\text{Fe}_2\text{O}_5$ require the introduction of a constant phase element (CPE) to explain the deviation of pure capacity [14]. A roughness factor ($n = 0.8$) is calculated by the relation (10):

$$n = 1 - \frac{2 \times \beta}{\pi} \tag{10}$$

Photocatalysis

As mentioned above, one of the best characteristics of colored perovskites is the high energetic position of the conduction band, deriving from $3d$ metal and a narrow gap sensitive to visible light, two attractive properties in the solar energy conversion. In this respect, hydrogen is an ideal fuel because of its cleanliness, renewability and heat combustion per unit mass and its production from the solar energy remains a challenging alternative [26, 27]. As application, the brownmillerite was successfully experimented for the H_2 photo-production; the evolved volume on $\text{Ca}_2\text{Fe}_2\text{O}_5$ was studied in aqueous

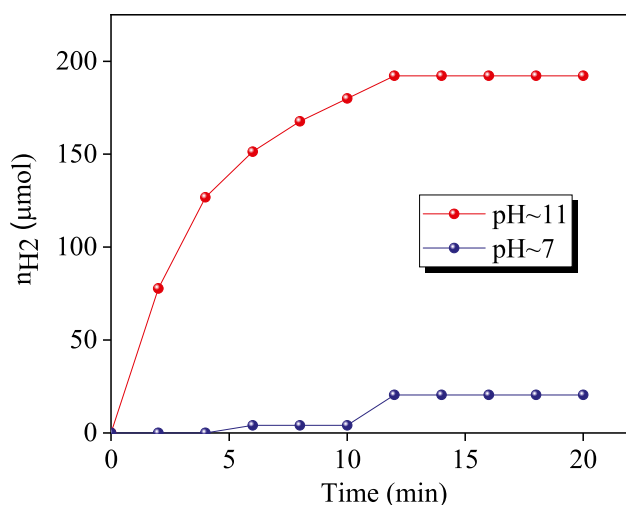
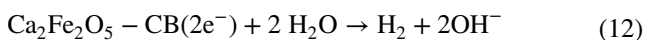
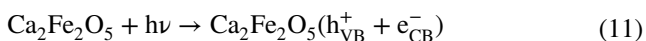


Fig. 8 Volume of evolved H_2 vs. illumination time over $Ca_2Fe_2O_5$ for pH~11 and pH~7

solution at two pHs (Fig. 8). The best performance was obtained in basic medium and this can be explained as follows: as pH increases from 7 to 11, the H_2O/H_2 level which varies by ~ -0.6 V/pH approaches the conduction band and reaches an band bending of ~ 0.25 V, equal to $(E_{H_2O/H_2} - E_{fb})$, close to the optimal value. This enhances considerably the electron transfer, thus producing a higher H_2 volume. It is worthwhile to outline that the oxide is chemically instable at high pH as shown by XRD analysis (SM 3). The water oxidation cannot occur by holes through a valence band (VB) process owing to the inadequate position of the couple O_2/H_2O (~ 1 V). This fact can be explained by the lowest band bending value ($E_{O_2/H_2O} - E_{fb} = \sim 0$ V).



The reproducibility of the $Ca_2Fe_2O_5$ was also investigated by conducting the cyclability tests up to two consecutive runs (Fig. 9).

The initial performance was restored with a deactivation of 20% after passing N_2 gas through the electrolytic solution, which reactivates the photocatalytic sites.

Generally, the specific surface area of the perovskites is low and the photoactivity can be limited by this parameter [28]. To increase the conversion yield, the brownmillerite was immobilized on different supports, namely the active carbon, zeolite [29], or combined with a wide band gap semiconductor (hetero-junction). Attempts to test our oxide in hetero-junction with ZnO are presently underway; the results are satisfactory and will be reported very soon. In addition,

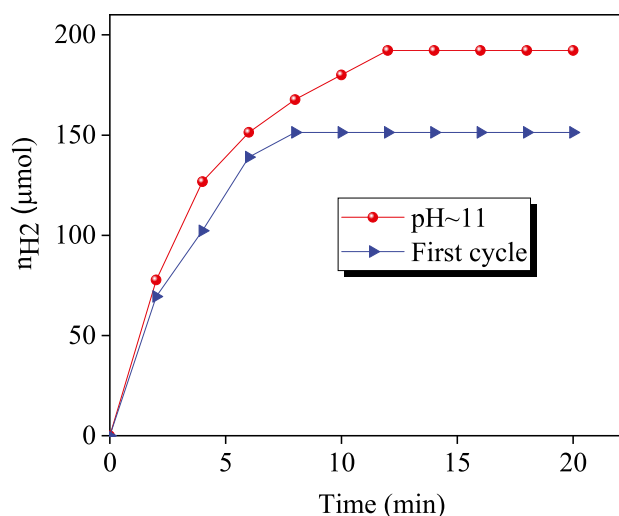


Fig. 9 Volume of evolved H_2 vs. illumination time over $Ca_2Fe_2O_5$ during two successive runs

to prevent the photocorrosion of $Ca_2Fe_2O_5$ and to enhance its photoactivity, the holes scavengers I^- and $Fe(CN)_6^{4-}$ will be also tested.

Conclusion

$Ca_2Fe_2O_5$ was successfully synthesized by citrate sol-gel auto combustion. The single phase, confirmed by XRD analysis, has been characterized by photo-electrochemistry for evaluation in the hydrogen production under visible light. The brownmillerite is classified as a narrow band gap semiconductor with a good stability over a wide pH range and suitable positions of the conduction band. The thermopower measurement indicated *p*-type conduction, a characteristic confirmed by the (capacitance-potential) plot. The exchange current density and the polarization potential in NaOH electrolyte are characteristic of a long-lived material. The electrochemical impedance spectroscopy showed the predominance of the bulk contribution and confirmed the semi conductivity. $Ca_2Fe_2O_5$ was successfully tested for the H_2 evolution upon visible light. Satisfactory results with ZnO will be reported in the future.

Supplementary information The online version contains supplementary material available at <https://doi.org/10.1007/s10008-022-05183-1>.

Acknowledgements The authors would like to thank Dr F. Touahra and Dr. A. Boudjemaa for numerous analyses.

Funding This work was supported by the Faculty of Chemistry (Algiers).

References

- Hammache Z, Soukeur A, Omeiri S, Bellal B, Trari M (2019) Physical and photo-electrochemical properties of MgFe_2O_4 prepared by sol gel route: application to the photodegradation of methylene blue. *J Mater Sci Mater Electron* 30(6):5375–5382
- Risch M (2017) Perovskite electrocatalysts for the oxygen reduction reaction in alkaline media. *Catalysts* 7:154
- Dimitrovska-Lazova S, Aleksovska S, Mirceski V, Pecovska-Gjorgjevich M (2019) Correlation between composition, electrical and electrochemical properties of $\text{LnCo}_{1-x}\text{Cr}_x\text{O}_3$ ($\text{Ln} = \text{Pr, Gd}$ and $x = 0, 0.5$ and 1) perovskites. *J Solid State Electrochem* 23(3):861–870
- Kanhere P, Chen Z (2014) A review on visible light active perovskite-based photocatalysts. *Molecules* 19(12):19995–20022
- Boudjellal L, Belhadi A, Brahim R, Boumaza S, Trari M (2018) Physical and photoelectrochemical properties of the ilmenite NiTiO_3 prepared by wet chemical method and its application for O_2 evolution under visible light. *Mater Sci Semicond Process* 75:247–252
- Dhankhar S, Bhalerao G, Baskar K, Singh S (2016) Synthesis and characterization of polycrystalline brownmillerite cobalt doped $\text{Ca}_2\text{Fe}_2\text{O}_5$. *AIP Conf Proc* 1731:5–8
- Boumaza S, Boudjellal L, Brahim R, Belhadi A, Trari M (2020) Synthesis by citrates sol-gel method and characterization of the perovskite LaFeO_3 : application to oxygen photo-production. *J Sol-Gel Sci Technol* 94(2):486–492
- Da Silva CC, Sombra ASB (2011) Temperature dependence of the magnetic and electric properties of $\text{Ca}_2\text{Fe}_2\text{O}_5$. *Mater Sci Appl* 02(09):1349–1353
- Hirabayashi D, Yoshikawa T, Mochizuki K, Suzuki K, Sakai Y (2006) Formation of brownmillerite type calcium ferrite ($\text{Ca}_2\text{Fe}_2\text{O}_5$) and catalytic properties in propylene combustion. *Catal Letters* 110(1–2):155–160
- Priyanga GS, Thomas T (2018) Direct band gap narrowing and light-harvesting-potential in orthorhombic In-doped- AlFeO_3 perovskite: a first principles study. *J Alloys Compd* 750:312–319
- Pailhé N, Wattiaux A, Gaudon M, Demourgues A (2008) Correlation between structural features and vis-NIR spectra of $\alpha\text{-Fe}_2\text{O}_3$ hematite and AFe_2O_4 spinel oxides ($\text{A} = \text{Mg, Zn}$). *J Solid State Chem* 181(5):1040–1047
- De Haart LGJ, Blasse G (1985) Photoelectrochemical properties of ferrites with the spinel structure. *J Electrochem Soc* 132(12):2933–2938
- Song S, Xu L, He Z, Ying H, Chen J, Xiao X, Yan B (2008) Photocatalytic degradation of C.I. Direct Red 23 in aqueous solutions under UV irradiation using $\text{SrTiO}_3/\text{CeO}_2$ composite as the catalyst. *J Hazard Mater* 152(3):1301–1308
- Wheeler GP, Choi KS (2018) Investigation of p-type $\text{Ca}_2\text{Fe}_2\text{O}_5$ as a photocathode for use in a water splitting photoelectrochemical cell. *ASC Appl Energy Mater* 1(9):4917–4923
- Boumaza S, Boudjemaa A, Bouguelia A, Bouarab R, Trari M (2010) Visible light induced hydrogen evolution on new hetero-system $\text{ZnFe}_2\text{O}_4/\text{SrTiO}_3$. *Appl Energy* 87(7):2230–2236
- Boumaza S, Brahim R, Boudjellal L, Belhadi A, Trari M (2020) Photoelectrochemical study of La_2NiO_4 synthesized using citrate sol gel method- application for hydrogen photo-production. *J Solid State Electrochem* 24(2):329–337
- Gowreesan S, Ruban Kumar A (2017) Structural, magnetic, and electrical property of nanocrystalline perovskite structure of iron manganite. *Appl Phys A* 123(11):689
- Omeiri S, Bellal B, Bouguelia A et al (2009) Electrochemical and photoelectrochemical characterization of CuFeO_2 single crystal. *J Solid State Electrochem* 13:1395–1401
- Bagtache R, Sebai I, Abdmeziem K, Trari M (2019) Visible light induced H_2 evolution on the hetero-junction Ag/NiO prepared by nitrate route. *Sol Energy* 177:652–656
- Asenath-Smith E, Lokuhewa IN, Misture ST, Edwards DD (2010) *p*-Type thermoelectric properties of the oxygen-deficient perovskite $\text{Ca}_2\text{Fe}_2\text{O}_5$ in the brownmillerite structure. *J Solid State Chem* 183(7):1670–1677
- Shaula AL, Pivak YV, Waerenborgh JC, Gaczynski P, Yaremchenko AA, Kharton VV (2006) *Solid State Ionics* 177(33–34):2923–2930
- Zhou HD, Goodenough JB (2005) Electronic behavior of three oxygen non-stoichiometric $\text{Fe}^{4+}/\text{Fe}^{3+}$ oxoperovskites. *J Solid State Chem* 178(12):3679–3685
- Tilley RJD (2004) in: *Understanding solids: the science of materials* John Wiley & Sons, England, Chichester, pp 363–390
- West AR (1984) in: *Solid state chemistry and its applications*. John Wiley & Sons, Chichester, England, pp 553–582
- Benamira M, Lahmar H, Messaadia L, Rekhila G, Akika FZ, Himrane M, Trari M (2020) Hydrogen production on the new hetero-system $\text{Pr}_2\text{NiO}_4/\text{SnO}_2$ under visible light irradiation. *Int J Hydrogen Energy* 45(3):1719–1728
- Boumaza S, Bouguelia A, Bouarab R, Trari M (2009) Physical and photoelectrochemical studies for hydrogen photo-evolution over the spinel ZnCr_2O_4 . *Int J Hydrogen Energy* 34(11):4963–4967
- Boudjemaa A, Rebahi A, Terfassa B, Chebout R, Mokrani T, Bachari K, Coville NJ (2015) Fe_2O_3 /carbon spheres for efficient photo-catalytic hydrogen production from water and under visible light irradiation. *Sol Energy Mater Sol Cells* 140:405–411
- Lam SM, Sin JC, Mohamed AR (2017) A newly emerging visible light-responsive BiFeO_3 perovskite for photocatalytic applications: a mini review. *Mater Res Bull* 90:15–30
- Jiang G, Lin Z, Chen C, Zhu L, Chang Q, Wang N, Wei W, Tang H (2011) TiO_2 nanoparticles assembled on graphene oxide nanosheets with high photocatalytic activity for removal of pollutants. *Carbon N Y* 49(8):2693–2701

Publisher's Note Springer Nature remains neutral with regard to jurisdictional claims in published maps and institutional affiliations.